IEEE Access
Multidisciplinary | Rapid Review | Open Access Journal

Received October 8, 2019, accepted December 26, 2019, date of publication January 6, 2020, date of current version January 15, 2020.

Digital Object Identifier 10.1109/ACCESS.2020.2964332

Fault-Tolerant Modular Stator Concentrated Winding Permanent Magnet Machine

ILYA PETROV[1], CHONG DI[1], PIA LINDH[1], MARKKU NIEMELÄ[1], ANNA-KAISA REPO[2], AND JUHA PYRHÖNEN[1], (Member, IEEE)

[1]Electrical Engineering Department, LUT University, 53850 Lappeenranta, Finland
[2]Rocla Oy, 04401 Järvenpää, Finland

Corresponding author: Ilya Petrov (ilya.petrov@lut.fi)

ABSTRACT This paper studies a modular permanent magnet synchronous machine (MPMSM) converted from a traditional single-core 24-slot 20-pole tooth-coil winding permanent magnet synchronous machine (TCW PMSM). The performance of the TCW PMSM is compared with the performance of the MPMSM (rearranged from this TCW PMSM) by the finite element method (FEM). It is found that if an electrical machine with a modular structure is designed, the efficiency of the MPMSM may be degraded compared with the conventional structure, especially, if a solid rotor yoke is used. However, the advantages of the proposed MPMSM are related to an option to scale up the machine by applying a certain number of modules, or removing faulty modules (while keeping the healthy modules working). This makes this type of a motor design applicable in certain life-critical applications, or in applications where scaling of the motor power might be needed. As a prototype, a low-power, low-speed generator added to a hook block of a hoist to supply power to measurement electronics is studied.

INDEX TERMS Permanent magnet machines, modular PMSM, TCW PMSM, tooth-coil winding.

I. INTRODUCTION

Differentfault-tolerant solutions are proposed in the literature for special applications such as air space or certain propulsion motor systems. Traditional merits to achieve these solutions are related to increasing number of phases [1], applying thermally and electromagnetically isolated modules for independent operation of each module [2], using electrically magnetized structure (e.g. switched reluctance motors) [3] or synchronous motors with high self-inductance [4] to avoid large continuous currents and braking torque in case of short circuit faults in the coil. However, the major development trend in the development of fault-tolerant electrical machines is often associated with a modular stator structure [5]–[7]. Indeed, a modular stator structure helps in reducing the mutual magnetic coupling between the phases and makes the stator phase windings more thermally isolated from each other. Furthermore, a modular stator structure makes it possible to remove faulty modules and continue to operate with the rest of the modules under partial load. This arrangement can also be applied to scale (discretely) the machines to fit certain power levels without modifying their geometry but only by removing modules belonging to one or more base machines in linear or rotating motors. Here, the term 'modular structure' refers to completely magnetically isolated stator modules (except for possible small flux leakages) as for example in [8]–[10], which is opposite to the quasi-modular structure where the air gap between the modules is unwanted and appears only as a result of certain stator segmentation (e.g. to simplify the assembly process). Such motors can be, in principle, referred to as traditional monolithic motors with parasitic air gap between the segments (modules) [11], [12].

In [8], 12-slot TCW PMSMs with 10-pole and 14-pole rotors were rearranged to have a modular stator, which consists of six modules. However, cutting was not made in the stator yoke but in the middle of the stator teeth. In [9], it is shown that a conventional 12-slot 10-pole TCW PMSM can operate with air gap barriers in the stator yoke, which splits the stator into six segments. In [9], the segment has a U-shape core structure, whereas in [8], the segment has an E-shape core structure. Therefore, with the E-shape core structure, only the single-layer winding is available, because otherwise it would require a winding between two neighboring segments, which easily ruins the idea of the modular structure. With the same logic, the U-shape core arrangement should resemble the double-layer winding. A topology similar to the

The associate editor coordinating the review of this manuscript and approving it for publication was Christopher H. T. Lee.

U-shape core structure is described in [13]. However, it has a nonfully isolated modular structure, only with certain flux barriers on the stator side in order to adjust the current linkage waveform caused by the armature winding.

In [14], [15], a flux-switching PM motor is described, which has a modular stator structure where permanent magnets are located between the stator segments. A single independent stator segment can comprise a U-shape core or an E-shape core [16]. However, the stator coils are wound around two cores and one magnet, which should be attached together as tightly as possible. It complicates the manufacturing with such a stator construction; further, an additional housing is needed [17].

The fault-tolerant motor proposed in this paper contains electromagnetically and thermally isolated segments. Part of these segments can be removed if needed while the rest of them can still continue working keeping the motor in operation. Because the rearranged machine enables removing faulty segments it allows to consider the machine as a fault-tolerant one. Other parameters of the proposed motor that have certain relation to fault tolerant capability (such as back EMF, electrical frequency and synchronous inductance) remain almost the same. The goal of the paper is to show the performance difference between the conventional monolithic motor and the motor rearranged from it (containing modular structure). Additionally, changes in the characteristics of the motor were analyzed at various loads using different number of independent modules. To the authors' best knowledge, the proposed motor has at least the following differences compared to previously proposed designs of modular PMSMs:

- open slots,
- asymmetrical position of the stator teeth,
- possibility of completely removing certain set of modules keeping the motor under the operation,
- independent winding of each module having end winding in normal direction, and
- outer rotor construction.

The outer rotor construction was selected to simplify the rotor integration to the hook block of a hoist where the designed machine was applied as a generator to supply some measurement electronics. However, the theory presented in the paper is also applicable to an inner rotor construction as well as to an axial flux arrangement and linear motors.

The challenges and certain limitations (related to the performance characteristics) of the modular stator structure are considered. The paper is organized as follows. In Section II, the overall constructional features of the MPMSM are described, and a comparison between the original and proposed arrangements is shown. Section III describes the advantages of the proposed modular stator structure and compares the performance of the MPMSM applying different sets of stator modules. Section IV verifies the simulated results with the assembled and tested MPMSM. Section V concludes the results.

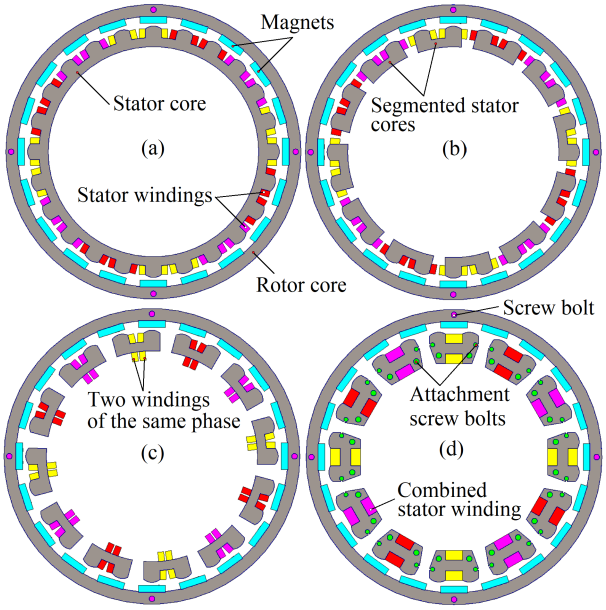

FIGURE 1. Geometry rearrangement of a monolithic stator with double-layer winding (a) into a segmented stator with half the number of segments compared with the slot number of the original stator (b); (c) Modular stator with the proposed single-layer winding arrangement; (d) Final design with modified shape of the segment (for simpler assembling procedure) and with an increased slot width inside the segment.

II. ELECTROMAGNETIC PARAMETERS OF THE MODULAR 24-SLOT 20-POLE PMSM AND ITS COMPARISON WITH A MONOLITHIC ARRANGEMENT

A segmented stator, which consists of separate modules magnetically totally isolated from each other, can be obtained by cutting the stator yoke. There are two possible ways to cut the stator yoke:

- when a segment includes only one phase and
- when a segment includes windings of two phases.

It is advantageous to have only one phase in a segment because of the better fault tolerance and easier mechanical assembly. In this case the original stator yoke, Fig. 1 (a), should be rearranged with the cuts in places shown in Fig. 1 (b). With such an arrangement there is only one phase per segment. Fig. 1 (c) shows another winding arrangement where the windings (originally locating outside of the inner slot of the segment) are positioned around of the yoke. Further, Fig. 1 (d) shows the final design of the proposed segmented solution. Extra modifications in this design are related with increased inner slot area of the segment. Also, extra holes (for stator core fixing) in each segment are added (green color in Fig. 1 (d)). Smaller holes are for tightening of the core laminates to each other and larger holes are for fixing of the segment to the common stator body frame.

By applying the cuts in the monolithic structure the magnetic state of the original machine is significantly modified as it is shown in Fig. 2. In Fig. 2 (a) it can be seen that the magnetic flux in the original machine is somehow evenly distributed within the rotor and stator yokes. However, when

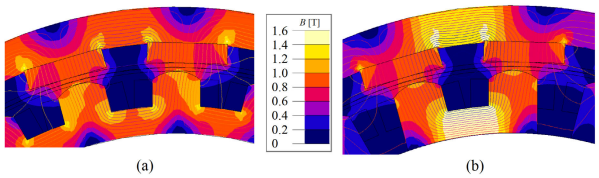

FIGURE 2. Flux density distribution at no-load in a) Original monolithic machine; b) Machine with cuts in the stator yoke. The rotor has a position when the phase of the shown machine region is having zero back EMF (maximum magnetic flux penetrating through it). 2D FEM.

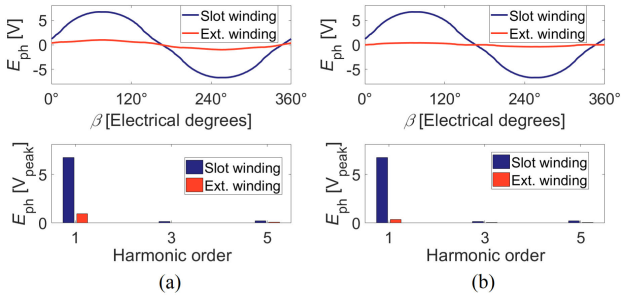

FIGURE 3. a) Phase EMF in the slot proportion of the winding and in the winding proportion located outside of the segment slot (behind the yoke) in the arrangement illustrated in Fig. 1 (b); b) phase EMF in the slot winding and in the winding located outside of the segment slot in the arrangement illustrated in Fig. 1 (c). Angular speed is 26.9 rpm (which is the rated speed of the hook block of a hoist). 2D FEM.

the cuts in the stator yoke are applied the magnetic flux concentrates in the remaining stator yoke regions. These regions have almost double peak flux density in comparison with the original monolithic design. Whereas, obviously there is no significant magnetic flux in the regions where the stator yoke has been cut away (replaced with air in the model). This means that the winding located inside of the slot in the segment should generate almost double back EMF compared with the same winding in the original monolithic stator. However, at the same time the winding which is located outside of the segment slot (behind the yoke) should generate much smaller back EMF, because the flux penetrating this winding is only comprised from the leakage flux between two neighbouring segments. This is verified by a back EMF waveform generated solely by segment slot winding and solely by the winding located outside of the segment slot as shown in Fig. 3 (a). The phase back EMF generated in the segment slot is 6.76 V_{peak} which is 85% of the total phase back EMF of the original monolithic machine. The phase EMF generated in the winding proportion outside of the segment slot is only 0.95 V_{peak} which is 12% of the total phase EMF of the monolithic design. Consequently, it can be claimed that the actual positioning of the winding outside of the segment slot does not lead to a large variation of the overall back EMF.

The overall back EMFs of all machine versions comprising the original monolithic machine (a), stator cut version with original winding positioning (b), stator cut version with rearranged winding positioning (c) and the final design version

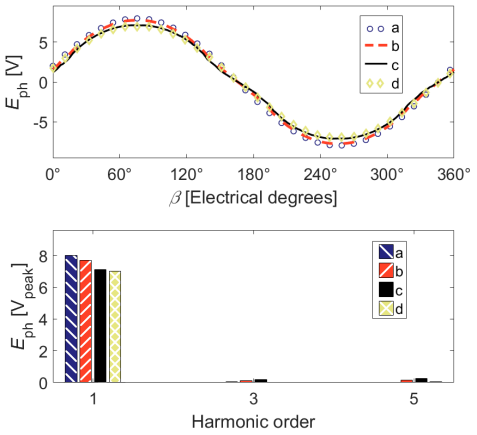

FIGURE 4. Back-EMFs of the 24-slot 20-pole PMSMs with different stator constructions (a–d) illustrated in Fig. 1 having the same number of stator turns in series per phase at no-load point with a rotational speed of 26.9 rpm. 2D FEM.

(c) are shown in Fig. 4. The fundamental harmonic of the back EMF of the original monolithic machine is 8 V_{peak}. When the cut in the yoke is applied the fundamental back EMF is reduced by 3.5% generating 7.72 V_{peak} of back EMF at the same speed. In case of rearranged winding position the back EMF is reduced by 11.2% compared with the original design generating 7.11 V_{peak} of back EMF. The final design including extra modifications for easier winding routine and fixation of the stator core is having 7.01V_{peak} or 87.5% of the back EMF generated in the original monolithic design.

In a segmented solution each segment creates a completely independent unit with minimum electromagnetic and thermal impact on other segments. However, the reduction of the back EMF in the proposed structure is the adverse phenomenon when the monolithic machine is converted into a segmented solution. On the other hand, if the winding positioning is not changed and remains as in the original machine structure after the stator core cut being applied as in Fig. 1 (b), then the back EMF reduction is only 3.5%.

A more detailed comparison of the original monolithic structure with two modular versions is obtained (keeping number of turns and phase resistance the same). Fig. 5 shows the torque as function of phase current and consequent efficiency of the machines at rotational speed of 26.9 rpm. The synchronous inductance of all three machines is almost the same. Therefore, the torque of the machines follows the same difference as the back EMF (found above). It means that the torque of the machine with cuts in the yoke and the torque of the final design is 96.5% and 87.5% of the torque of the original monolithic machine respectively. The efficiency curves show a similar trend. It is shown that if only cuts in the stator yoke are applied there is no essential drop in the efficiency, whereas the efficiency drop of the final design is more evident. However, in this paper just a concept of the proposed fault tolerant solution is described and for easier manufacturing of the concept the final design was obtained

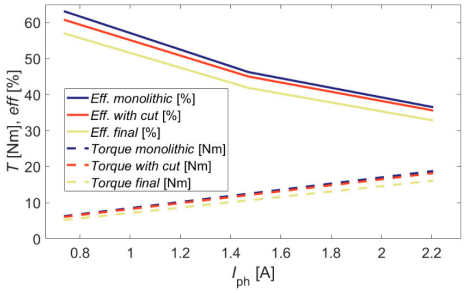

FIGURE 5. Torque and efficiency as function of applied current in the original monolithic motor, in the motor with applied cuts in the stator yoke (keeping the winding position unchanged), and in the final design case. Rotational speed is 26.9 rpm. 2D FEM.

as in Fig. 1 (d). The parameters of the designed PMSM are introduced in Table 1. The main size parameters of the machine listed in Table 1 were adjusted for the integration of it in the pulley of a hook block of a hoist.

TABLE 1. Parameters of the final machine design.

Parameter	Value
Stack (physical) iron length l_{Fe} [mm]	38
Stator inner diameter D_{si} [mm]	138
Stator outer diameter D_{so} [mm]	187
Rotor outer diameter D_{ro} [mm]	219
Air gap length δ [mm]	2
Number of stator segments Q_{segm}	12
Number of pole pairs p	10
Permanent magnet height [mm]	5
Winding connection	star
Stator core material	M400-50A
Rotor core material	Fe52
Rated speed n [rpm]	227
Phase resistance R_{ph} [Ohm]	6.3
Rated voltage V_{ph} [Vrms]	49
Rated current A_{ph} [Arms]	1.4
Rated torque T [Nm]	5.8
Rated power P [W]	138
Synchronous inductance L_{s} [H]	0.02

The cogging torques of the machines (shown in Fig. 1) with a solid rotor made of constructional steel S355 and laminated nonconducting rotor are illustrated in Fig. 6. In Fig. 6 (a) it can be seen that the stator segmentation (cutting it into independent modules) in the case with solid rotor makes the negative DC torque component (against the rotor rotation) more evident. This can be explained by the flux variation in the rotor core at different rotor positions which generates extra eddy currents in the solid rotor, as it is shown in Fig. 7. Further, in Fig. 6 it can be seen that the 6$^{\mathrm{th}}$ harmonic component appears when the cut is applied in the stator yoke. It can be explained by the presence of the 6$^{\mathrm{th}}$ harmonic component in a single segment torque profile as can be seen in Fig. 8 (a). The cogging torque spectrum analysis showed that there are some even harmonics present. However, most of them are cancelled when two other segments are added, Fig. 8 (b). Therefore, there are only the 6$^{\mathrm{th}}$ and the 12$^{\mathrm{th}}$ harmonics left in the complete base machine (comprising at least three segments).

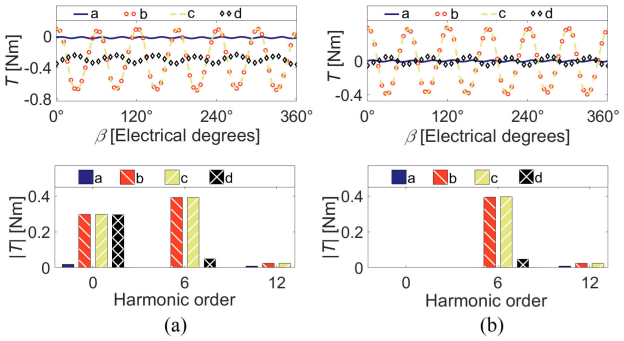

FIGURE 6. Cogging torque with different stator constructions (a–d) illustrated in Fig. 1 when a) Rotor core is made of solid constructional steel S355; b) Rotor core is made of standard lamination. The rotational speed is 26.9 rpm. 2D FEM.

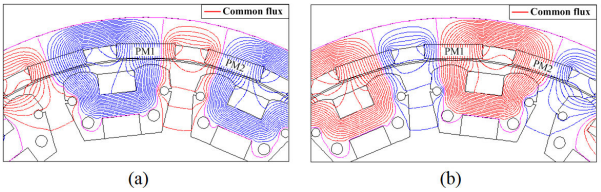

FIGURE 7. Flux pattern variation in different positions of the stator relative to the rotor at no-load. Position of the stator changes while the rotor position remains the same to highlight how the magnetic flux varies within the rotor yoke. a) Position when the common flux between permanent magnets PM1 and PM2 is at minimum. b) Position when the common flux between permanent magnets PM1 and PM2 is at maximum. 2D FEM.

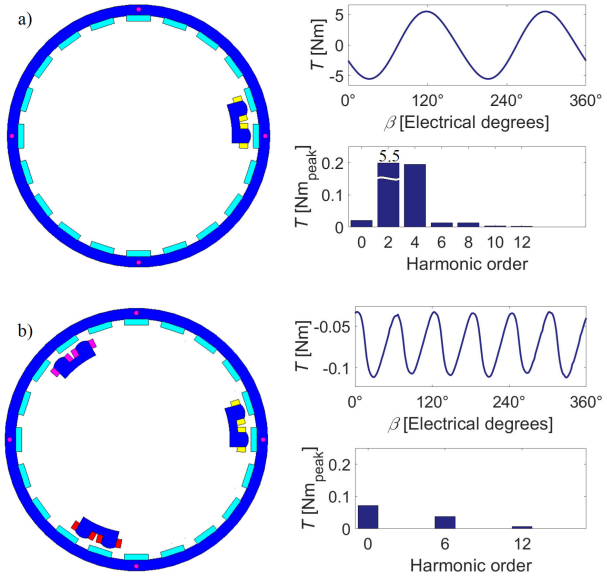

FIGURE 8. Structure and cogging torque of a) Machine having one single module; b) Machine having three segments evenly distributed within the stator periphery with overall electrical angle multiple to 120 electrical degrees. The rotational speed is 26.9 rpm. 2D FEM.

In Fig. 6 it can be seen that the final design has a much smaller 6$^{\mathrm{th}}$ harmonic compared with the cogging torque of initial modular PMSM design cases. This was achieved by an adjustment of the slot width in the final design case. It should

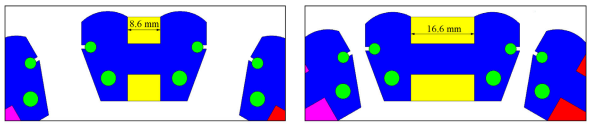

FIGURE 9. Variation of the slot width in the segment.

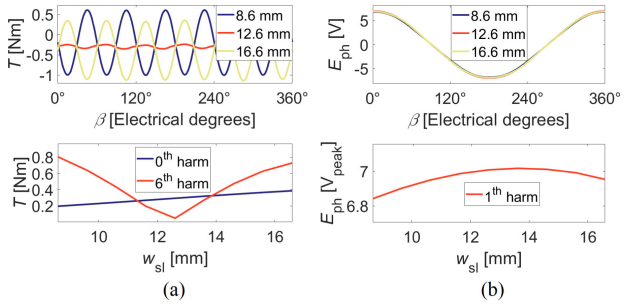

FIGURE 10. a) Cogging torque and variation of its DC component with the 6^{th}-order harmonic as function of slot width of the final modular PMSM design; b) Back EMF and variation of its fundamental harmonic as function of slot width of the final modular PMSM design. 2D FEM.

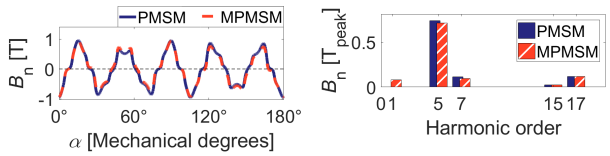

FIGURE 11. Air gap flux density waveforms and their spectra, in the normal direction of the MPMSM, and the PMSM illustrated in Fig. 2. 2D FEM.

be noted that when the slot width of the segment is varied there is no need to reduce the stator tooth width as it would be in the case of a monolithic stator. In case of segmented stator it is possible to change the slot width by modifying only the distance between the segments as it is shown in Fig. 9. The cogging torque and back EMF at different slot widths are shown in Fig. 10. The minimum cogging torque is found when the slot width is 12.6 mm which is 5% larger than the initial slot width. The back EMF also has the highest value at about the same slot width proportion.

A rotor yoke in outer rotor PMSMs can be made of solid steel to improve robustness and simplicity [18]. However, in TCW PMSMs there is a wide range of harmonics in the air gap current linkage spectrum [18], [19], which leads to significant losses in the rotor yokes made of solid steel. These losses are the price one has to pay when using a simple rotor construction together with a TCW. Further, the stator segmentation increases these losses because of the permeability variations seen by the rotor in different positions. These permeability variations cause alternation in the magnetic flux value in the rotor yoke as illustrated in Fig. 7. Therefore, it is not advisable to use modular electrical machines of this kind in an application that requires a high rotational speed. Otherwise, it is advisable to use a laminated rotor yoke (not solid steel) to keep the rotor losses at an acceptable level.

The proposed segmented solution has an effect on the air gap flux density distribution. The flux density for machines illustrated in Fig. 2 (a) and (b) in the normal direction can be seen in Fig. 11. The flux densities in the tangential direction are not shown for limited space reasons. However, they are even more similar to each other than the flux densities in the normal directions. In Fig. 11 it is seen that the 5^{th} flux density harmonic (the operating flux density harmonic within 180 electrical degrees) is only 3.5% lower than that of the conventional TCW PMSM which is matching the back EMF results derived above.

TABLE 2. Comparison of the original monolithic machine structure with final design of modular machine structure at 26.9 rpm and 1.4 Arms phase current.

Parameter	Original monolithic	Proposed segmented
Back EMF (26.9 rpm) $E_{\mathrm{ph.peak}}$ [V]	8 (1 pu)	7.01 (0.875 pu)
Nominal torque (1.4 Arms) T_{n} [T]	6.63 (1 pu)	5.8 (0.875 pu)
Cogg. torque $T_{\mathrm{cogg.p2p}}$ [Nm]	0.02	0.1
Efficiency (26.9 rpm, 1.4 Arms)	20%	18%
Scalability	None	1/4:1/3:1/2:1
Winding routine	+	++
Fault tolerance	+	++

Table 2 shows comparative results of the original monolithic machine structure and of the proposed modular machine structure. Based on the results it can be additionally stated that the modular structure may suffer from some reduction in performance compared with the monolithic structure. However, based on [20] the performance of the modular machine structure can be improved by using extra flexibility of the segmented stator arrangement (e.g. applying tooth tips between the segments that do not ruin the simple winding routine).

III. SCALABLE CAPABILITY AND PERFORMANCE OF THE MPMSM

Based on the results of the electromagnetic analysis, it can be concluded that in terms of back EMF and torque density, the electromagnetic performance of the modular PMSM structure described in this paper is inferior to the conventional PMSM. However, the proposed modular structure has certain advantages over the monolithic structure. Along with fault tolerance and scalability (which are described below), it has only half of the coils compared with the monolithic stator with a double-layer winding (the number of turns per phase is the same) and a simpler winding routine.

The modular structure with magnetically isolated coils allows to significantly reduce the magnetic coupling between the coils. This means that a fault of one coil does not impact other coils located nearby. Therefore, if each segment (coil) is controlled independently with the proposed modular stator structure or parallel connection of the coils in one phase is arranged, in the case of a fault it is possible to switch off the faulty coil keeping the machine operating by other coils.

Moreover, with the proposed modular stator structure, by using independent control of each coil in the case of a short-circuit in one coil, it is possible to remove only the

fault module with the other modules comprising the same base machine (to avoid magnetic unbalanced pull force in the radial direction) and continue operation using the remaining healthy coils. In this case, the coil which is in short-circuit after being removed does not produce magnetic force that opposes the operating mode. The possibility of removing one or more base machines can be accomplished by controlling each base machine separately (which increases the cost of the control) or connecting of each base machine in parallel (as all base machines have identical back EMF).

Another approach if a machine consists of two or more base machines is the option to switch off one base machine in the case of a fault or keep it as a spare one (nonactive) while the other base machine(s) is (are) operating for the sake of redundancy. While the machine is using at least one base machine it is possible to remove and perform maintenance work with the spare base machine(s). The analyzed PMSM has 24 slots and 20 poles, comprising two 12-slot 10-pole base machines [21]. However, one base machine has two separate symmetrical 3-phase winding systems. Therefore, only half of the slots (six coils) in one base machine constitute a fully independent 3-phase winding [22]. This means that by using the same rotor (track side in the case of a linear MPMSM) having ten poles, it is possible to get two independent sets of stator modules with a symmetrical 3-phase winding system. This leads to four independent sets of stator modules in the studied 24-slot 20-pole MPMSM. Hereafter, each set of modules (containing three modules) is designated as a base machine.

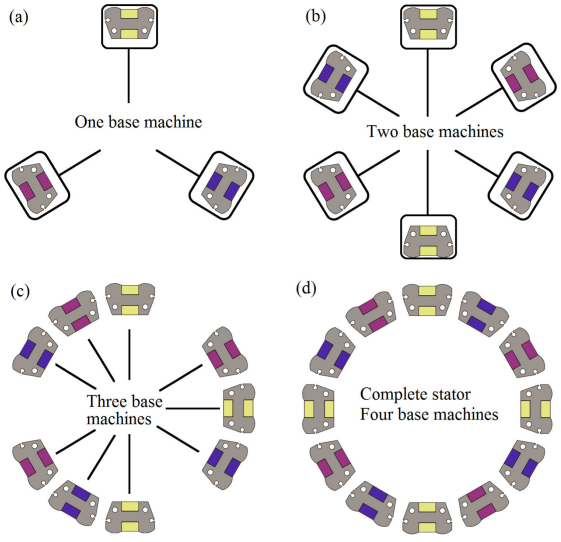

FIGURE 12. Possible sets of stator modules with a) one base machine; b) two base machines; c) three base machines; d) four base machines that comprise the stator. The base machines can be relatively independent of each other if they have a parallel winding connection.

Fig. 12 shows alternative sets of stator modules that have a symmetrical 3-phase winding system as well as symmetric distribution of normal force relative to the rotor center axis, which avoids problems with bearings or extra vibrations [23]. By having 24 slots in total it is possible to have four different sets of stator modules with one, two, three, and four base machines. If the base machines are connected in parallel and have the same number of turns, then, in each case, the back EMF would be the same. The parallel connection of the base machines using the same number of turns is a must if an option with switching off or removing of certain number of base machines is required to maintain the same voltage level. Naturally, in this case the current density in the remaining base machine(s) would be higher if one or more base machines are removed. This proposes that the machine cannot operate for a long time period with the remaining base machines alone because of a risk of overheating. Otherwise, if the machine must tolerate a long working period using only some of the base machines then they need to be initially somehow over dimensioned.

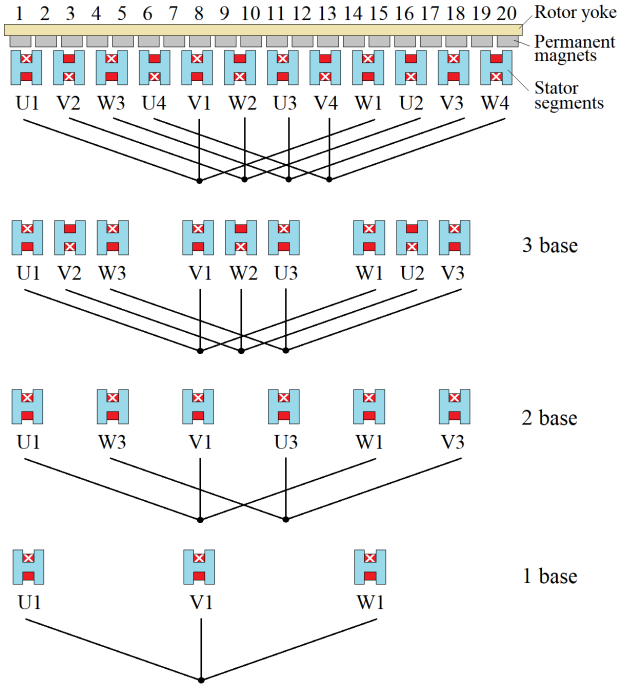

FIGURE 13. Positioning of the segments to comprise one or several complete base machines and a proper connection to avoid unbalanced magnetic pull and extra cogging torque. All the base machines can be connected in parallel as they are completely identical in terms of phase shift and amplitude of the generated back EMF. White crosses show the beginning of a coil.

Fig. 13 shows the connection of the segments that should comprise a 3-phase symmetrical arrangement without introducing extra magnetic pull to the bearings when applying different number of base machines. For the original nachine type the segment pitch $\tau_{\text{segm.}}$ and the pitch between two phases $\tau_{\text{ph.base}}$ in one base machine (to avoid any extra magnetic pull force while using any number of base machines) can be found as

$$N_{\text{segm.}} = 3N_{\text{base}} = mqp, \tag{1}$$

$$\tau_{\text{segm.}} = \frac{D_s \pi}{N_{\text{segm.}}}, \tag{2}$$

$$\tau_{\text{ph.base}} = N_{\text{base}} \tau_{\text{segm.}}, \tag{3}$$

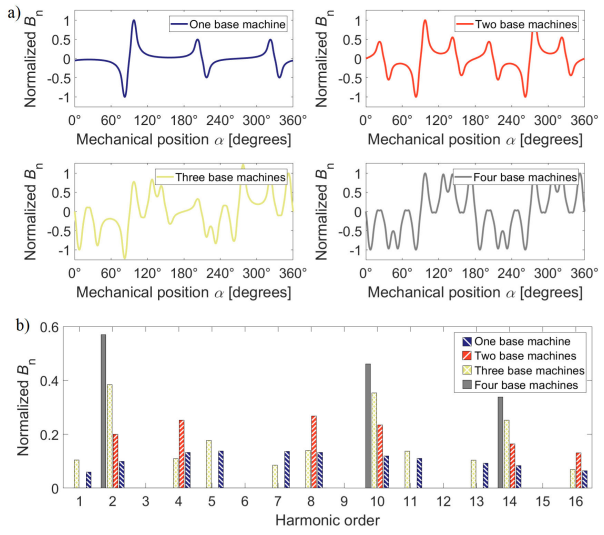

FIGURE 14. a) Normalized air-gap flux density waveforms generated from the stator winding excitation; b) Spectra of the normalized air-gap flux density. 2D FEM.

where $q = 0.4$ is the number of slots per pole and phase, N_{base} is the maximum number of possible base machines, $N_{\text{segm.}}$ is the maximum number of segments, m is the number of phases, p is the number of pole pairs, D_s is the stator diameter (outer stator diameter in case of inner stator).

Fig. 14 shows the normalized air-gap flux density (per-unit air-gap flux density) waveforms and the corresponding spectra generated from the stator winding excitation for all the four base machines. Typically, the current linkage (or magnetomotive force) is utilized to evaluate the stator winding performance. The situation becomes much more complex because of the special modular stator and the nonuniform distribution of air-gap length. Consequently, the normalized value of the air-gap flux density is chosen since it precisely takes both the current linkage and air-gap permeance into consideration. The peak flux density of four base machines is taken as a reference value for normalized flux density in all cases. The 10^{th}-order harmonic (working harmonic) amplitudes in Fig. 14 from one base machine to four base machines are 0.46, 0.35, 0.23, and 0.12, respectively. The ratio between these harmonic amplitudes is about $1 : 1/2 : 1/3 : 1/4$, which indicates that if a single base machine should produce the same torque as four base machines the current density in the single base machine should be quadruple compared to the four-base-machine case. This information also reveals that at the same load Joule losses in the stator winding increase with less number of operating base machines. Besides, it can be also seen in the figure that the machines have some additional sub-harmonics and high order harmonics. These harmonics cause extra rotor eddy-current losses. It can be concluded that applying less base machines might cause wider spectum of sub-harmonics because of larger distances between adjacent segments. For example, four base machines have the least number of harmonics (only 2^{nd}, 10^{th} and 14^{th} within the analysed range). However, the amplitude of these harmonics is a multiple of the number of base machines applied (similarly as with the working 10^{th} harmonic described above). Reducing the number of base machine by half (from four to two) generates extra even harmonics (2^{th}, 8^{th} and 18^{th}). Further, if the number of base machines is odd (e.g. 1 or 3) it generates extra odd harmonics (1^{st}, 5^{th}, 7^{th}, 11^{th} and 13^{th} within the analysed range).

Except the rotor eddy-current losses induced from the stator harmonics, the rotor flux alternation as shown in Fig. 7 is also capable of generating rotor eddy-current losses. This type of loss can be distinguished from no-load cogging torque, which can be evaluated directly from the torque curves analysis in Fig. 15. It can be seen that the cogging torque curves in Fig. 15 (a) for each set of stator modules have two major components: the DC component and the 6^{th}-order harmonic. The DC components represent the eddy-current losses (DC component torque times the rotational speed, 0.22 W, 0.37 W, 0.65 W, and 0.83 W, respectively from one base machine to four base machines) generated in the solid rotor, which is at smallest when only one base machine is applied and increases with two and more base machines. This can be explained by the interaction of the smaller number of stator modules (in the case of one base machine) with the rotor, and as a result, less magnetic flux variation in the rotor, which induces less eddy currents. Naturally, also the stator iron losses are smaller when a low number of stator modules is used. However, with a larger number of base machines (if they have parallel winding connections), the phase resistance reduces in inverse proportion to the number of base machines. This leads to a consequent reduction in the winding Joule losses (having the same phase current). Therefore, an optimum number of base machines in the stator can be selected based on the lowest total losses, with a trade-off between rotor and stator iron losses and winding Joule losses.

In Fig. 15 (b) torque curves are shown when 2.94 Nm load torque is applied. High-order harmonics in the torque ripple curve have similar trend as those harmonics in the cogging torque curve. Further, a higher current should be applied when the number of base machines is reduced if the same load torque remains as it was discussed earlier. However, the current increase with a lower number of operated base machines is not linear as it would be expected from the linear drop of the operating harmonic with lower number of applied base machines (illustrated in Fig. 14). The reason of that is different rotor loss components that act against the induced torque. For example, when one, two or three base machines are used instead of full stator (four base machines) the current in the coils is increased by 363%, 87.3% and 28.4% respectively. Whereas, it would be expected to have a current increase by 400%, 100% and 33.3% respectively. In any case the difference in the supplied current to keep the same torque value applying a lower number of base machines is significant. This means that either the machine needs to be oversized operating at the nominal load or operation time

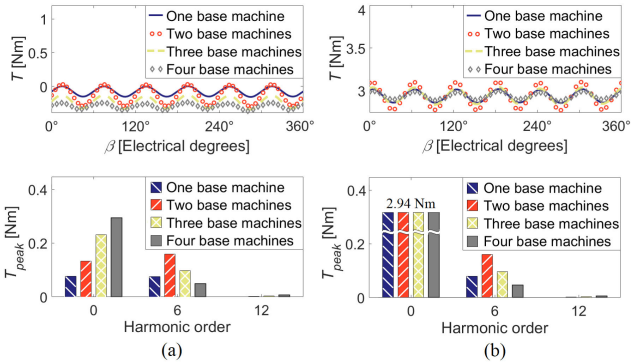

FIGURE 15. a) Cogging torque; b) Torque ripple (at 2.94 Nm load torque) for different sets of stator modules (shown in Fig. 12) with solid conducting rotor at a rotational speed of 26.9 rpm. 2D FEM.

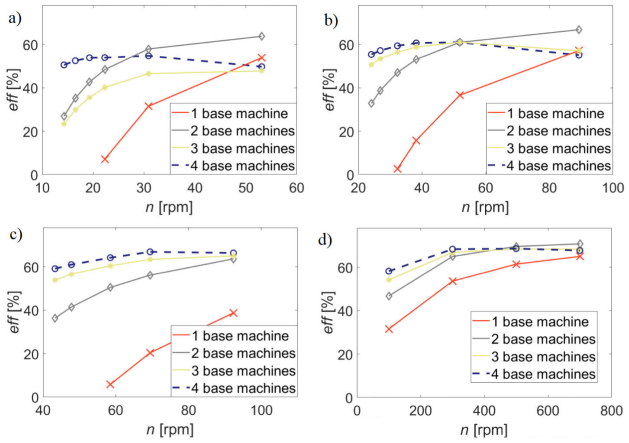

FIGURE 16. Estimated efficiency of the machine in the generator mode (with purely resistive load) as function of speed with (a) $T = 1.18$ Nm, (b) $T = 1.77$ Nm, (c) $T = 2.94$ Nm, (d) Efficiency in the motor mode ($i_d = 0$ control) $T = 7.8$ Nm as a function of speed of four different sets of stator modules. 2D FEM.

at faulty condition (when less number of base machines are used) should be limited.

If it is assumed that the synchronous inductance of the machine (in per units) is much smaller than the phase resistance, which can happen in a low-speed rotor surface magnet machine with a moderate tangential stress value, the maximum power of the machine is defined by this phase resistance. For example, if this machine is operating as a generator with a purely resistive load, the maximum power occurs when the resistance of the load equals the resistance of the machine. Therefore, if the windings of base machines are connected in parallel to keep the same voltage value (making the resistance in inverse proportion to the number of base machines), the number of base machines selected by a certain set of stator modules determines not only the loss distribution in the machine but also the maximum achievable power, which is a multiple of the number of base machines applied. The same is valid when the windings of the base machines are connected in series making the voltage value in the machine in proportion to the number of base machines.

However, the final decision about the optimal set of stator modules can be based on the efficiency level at a certain load. For example, by using different sets of stator modules it is possible to get different efficiency levels. Fig. 16 shows the efficiency of the MPMSM at four different torque values (1.18 Nm, 1.77 Nm, 2.94 Nm, 7.8 Nm) as a function of speed in the MPMSM with different numbers of base machines. Selection of these particular load points (1.18 Nm, 1.77 Nm, 2.94 Nm) is explained by the opportunity to verify the results by measurements having the same load points (discussed in the following section).

Fig. 16 (a) shows that at a lower torque and a higher speed, using a low number of base machines (one or two) allows to achieve higher efficiency because of the lower rotor core losses (which are dominant at a low torque and a high speed). However, at the low speed, when the proportion of stator winding Joule loss increases, a higher number of base machines (two, three, or four) should be applied as they provide higher efficiency. A similar trend can be observed in Fig. 16 (b), where the applied torque value is still moderate (1.77 Nm). However, in Fig. 16 (c) with the torque of 2.94 Nm, the MPMSM with three or four base machines has higher efficiency in the whole speed range, because of the high proportion of Joule losses at a high torque, which is amplified in inverse to the number of base machines (with a parallel winding connection).

It should be noted that there are only two major loss contributors at low speeds: the stator winding and the solid rotor core. Consequently, if the rotor core was made of a lamination stack, the rotor loss would be much smaller leading always to a higher efficiency at moderate rotational speeds when more base machines are applied. However, with an increase in rotational speed, the stator stack iron losses can reach the level of winding Joule losses, and in this case, selecting a lower number of base machines at certain loads might still lead to a higher efficiency.

Before making a decision about the number of base machines, also the thermal management of the configuration should be considered. For example, one base machine is more vulnerable in terms of local overheating as the Joule losses in the stator winding are higher (resulting from a higher phase resistance), and they concentrate on a smaller copper area. In the case of one base machine and a torque of 2.94 Nm (zero speed) the current density in one base machine is 10.6 A/mm^2 which is relatively high, whereas in the case of four base machines it is only 2.6 A/mm^2, this result matches the spectra of normalized air-gap flux density in Fig. 14 quite well. However, otherwise, if thermal management is not an issue for an application, a smaller number of base machines can be successfully applied at high speeds without a loss of operational power. Similarly, in an emergency, the reduced number of base machines can be used for a certain time period before the rest of the base machines are fixed and start to operate again.

IV. MEASUREMENT SETUP AND VERIFICATION OF THE SIMULATION RESULTS BY MEASUREMENTS

A prototype of the MPMSM was manufactured to operate as a generator in a hook block of a hoist and assembled to its pulley as shown in Fig. 17. The parameters of the machine are listed in Table 1.

The performance of the prototype, the geometry of which is shown in Fig. 1 (d), was measured in several points along the torque and speed axes. A simplified schematic arrangement of the test setup for the measurements is shown in Fig. 18 (a) and a photograph of the test setup bench in Fig. 18 (b). The generator is attached directly to the pulley. Thus, by rotating the pulley at a particular speed, the angular speed of the generator is known. The weight shown in Fig. 18 (a) was tuned to produce a particular force to the pulley, which together with its radius gives the torque needed for the generator, and at the same time, rotates the pulley at a particular speed (the angular speed depends on the weight and the generator load).

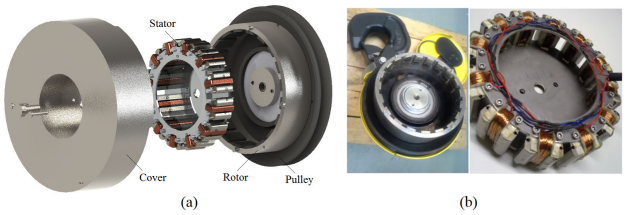

FIGURE 17. a) MPMSM assembly to the pulley; b) Rotor and stator assembled.

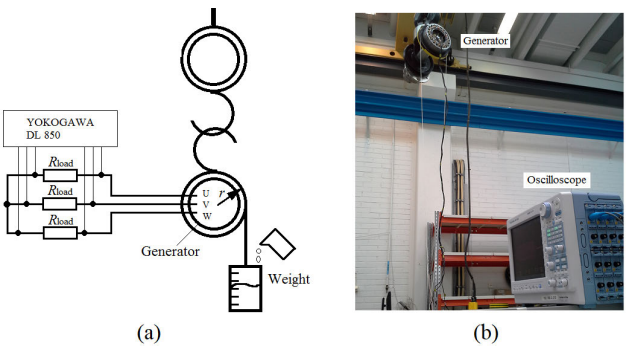

FIGURE 18. a) Simplified schematic arrangement of the test setup; b) Photograph of the test setup bench. The weight and the load resistances are not shown.

Therefore, the input power is known, being a multiple of torque and angular speed. The output power was regulated by varying the load resistances (R_{load}). The voltages at the terminals of the load resistances were measured at different loads (masses) of the generator. Three different masses, 1 kg, 1.5 kg, and 2.5 kg were used, producing shaft torques of 1.18 Nm, 1.77 Nm, and 2.94 Nm, respectively. Again, six different load resistances were implemented; 16.2 Ohm, 19.4 Ohm, 24.8 Ohm, 32 Ohm, 47 Ohm, and 100 Ohm. The variation in the mass and the load resistances yields 18 load points. When the mass is released, it starts to rotate the pulley. However, there is an acceleration time, as it is shown in Fig. 19 (a). The analysis of the results should be made in the steady state; Fig. 19 (b).

The voltage measured at the terminals in one particular operating point ($T = 2.94$ Nm, $n = 70$ rpm) is compared with the FEM-simulated voltage at the same resistive load and at the same angular speed. In both cases, the MPMSM operates in the generator mode. However, the measured MPMSM had a constant torque ($T = 2.94$ Nm), and thus, a particular speed is reached when the stator current is high enough to produce the same torque to reach the steady state. In the FEM simulation, the MPMSM was rotated at the same speed as the steady-state speed of the measured machine, and the output was the torque value. The resultant voltage curves of the measured and simulated FEM MPMSMs are shown in Fig. 20. It can be seen that the voltage curves coincide with each other, with an amplitude difference of only 2 %. However, the MPMSM simulated with the same load resistance had a slightly higher shaft torque (on average about 0.08 Nm). It can be explained by the additional mechanical friction torque, which is not taken into account in the simulation. The possible eddy currents induced at the end plates can also be an additional source of shaft torque reduction [24]. Therefore, in the final value of estimated torques, the value of 0.08 Nm (ca. 2% of the nominal torque) was added to compensate for these uncertainties.

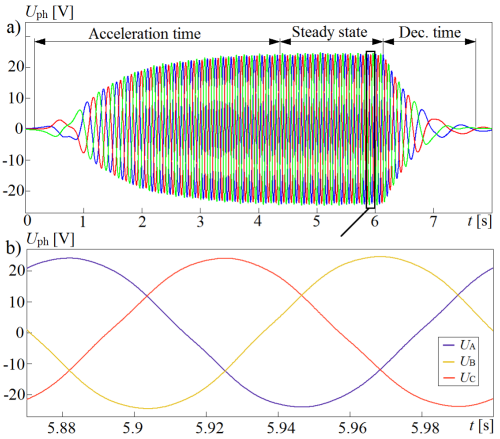

FIGURE 19. a) Measured voltage at the resistive load when the weight is released; b) One electrical period during the steady-state time of the measured voltage.

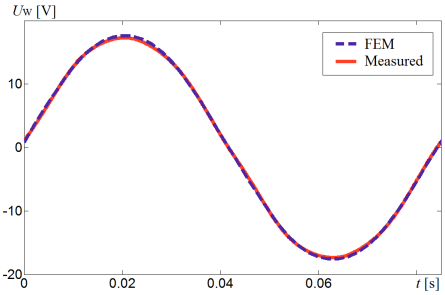

FIGURE 20. Measured and simulated voltage waveforms at the resistive load when the weight is released.

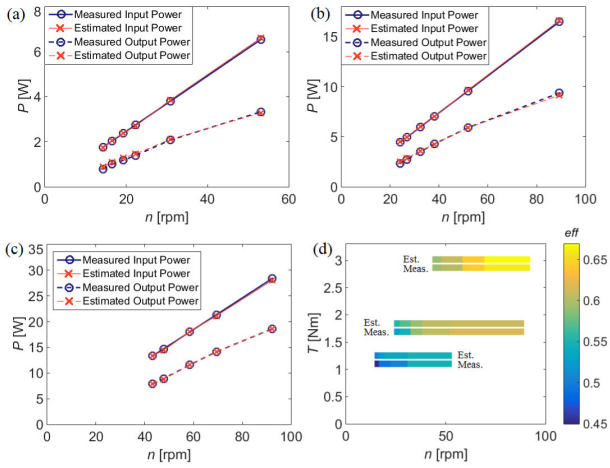

FIGURE 21. Measured and estimated input (mechanical) power and output (electrical with a purely resistive load) power at (a) $T = 1.18$ Nm, (b) $T = 1.77$ Nm, (c) $T = 2.94$ Nm as a function of speed; d) Measured and estimated efficiencies at the same torque values as a function of speed.

The purely active load in the test setup can reduce the output power because of the armature reaction [25]. However, the synchronous magnetizing inductance is relatively low in the MPMSM (in the range of 0.1 pu at the nominal load) because of the relatively low linear current density (electrical loading) and high effective air gap. The low synchronous magnetizing inductance leads to a low armature reaction of the MPMSM even at the maximum continuous load. This means that there is no significant output power reduction at a purely resistive load, as the highest current components stay on the q-axis.

If the value of the load resistances is known, by measuring the voltage at their terminals, it is possible to estimate the phase current, and consequently, the output power. This together with the input power provides an opportunity to estimate the efficiency at the measured load points. The input and output powers (estimated and measured) at different values of torque along with the estimated and measured efficiencies are shown in Fig. 21.

The losses that were included in the FEM analysis are the stator copper losses, the rotor solid yoke losses, the stator iron losses, and the permanent magnet Joule losses. It should be mentioned that the permanent magnet Joule losses and the stator iron losses are relatively low in the investigated machine in the observed operating points compared with the stator copper resistive loads and the rotor yoke losses, and do not significantly contribute to the total losses. The measured and estimated loads shown in Fig. 21 match quite well with the measured and estimated efficiencies. This verifies the validity of the simulation model used to estimate the motor performance.

V. CONCLUSION

The conventional 24-slot 20-pole PMSM was compared with a modular PMSM (rearranged from this PMSM) in terms of different performance aspects. The efficiency degradation in the MPMSM is mainly because of the additional solid rotor losses and a slightly lower back EMF. Therefore, the electromagnetic performance of the described modular structure is inferior to the conventional stator structure. However, the proposed segmentation of the PMSM has certain advantages which can be viable for special applications:

- operating the machine with faulty segments being removed,
- scalability (possibility to remove or add some of the base machines to achieve needed motor characteristics at certain load),
- strong thermal and electromagnetic decoupling between the segments to achieve high fault tolerance,
- more freedom in modification of the stator cores (e.g. increase slot width by changing the air gap between the segments without affecting the core tooth width),
- relatively simple winding routine.

Analysis of segmented motor performance using different number of base machines showed that it is possible to operate the motor with any number of base machines that comprise the complete stator. Cogging torque, torque ripple and unbalanced magnetic pull remain at the same level as in the complete stator. With the reduction of the applied base machines the winding Joule losses increase, while the rotor and stator core losses reduce.

REFERENCES

[1] L. Xu, G. Liu, W. Zhao, X. Yang, and R. Cheng, "Hybrid stator design of fault-tolerant permanent-magnet Vernier machines for direct-drive applications," *IEEE Trans. Ind. Electron.*, vol. 64, no. 1, pp. 179–190, Jan. 2017.

[2] L. Szabo and M. Ruba, "Segmental stator switched reluctance machine for safety-critical applications," *IEEE Trans. Ind. Appl.*, vol. 48, no. 6, pp. 2223–2229, Nov. 2012.

[3] M. Ruba, I.-A. Viorel, and L. Szabó, "Modular stator switched reluctance motor for fault tolerant drive systems," *IET Electr. Power Appl.*, vol. 7, no. 3, pp. 159–169, Mar. 2013.

[4] T. Raminosoa, C. Gerada, and M. Galea, "Design considerations for a fault-tolerant flux-switching permanent-magnet machine," *IEEE Trans. Ind. Electron.*, vol. 58, no. 7, pp. 2818–2825, Jul. 2011.

[5] T. Yao, W. Zhao, F. Bian, L. Chen, and X. Zhu, "Design and analysis of a novel modular-stator tubular permanent-magnet Vernier motor," *IEEE Trans. Appl. Supercond.*, vol. 28, no. 3, pp. 1–5, Apr. 2018.

[6] W. Ding, S. Yang, Y. Hu, S. Li, T. Wang, and Z. Yin, "Design consideration and evaluation of a 12/8 high-torque modular-stator hybrid excitation switched reluctance machine for EV applications," *IEEE Trans. Ind. Electron.*, vol. 64, no. 12, pp. 9221–9232, Dec. 2017.

[7] K. Wang, H. Lin, H. Yang, D. Wang, S. Fang, and Y. Huang, "Novel fault-tolerant stator structure for modular PMSMs with fractional-slot overlapping winding," in *Proc. 20th Int. Conf. Elect. Mach. Syst. (ICEMS)*, Aug. 2017, pp. 1–4.

[8] G. J. Li, Z. Q. Zhu, W. Q. Chu, M. P. Foster, and D. A. Stone, "Influence of flux gaps on electromagnetic performance of novel modular PM machines," *IEEE Trans. Energy Convers.*, vol. 29, no. 3, pp. 716–726, Sep. 2014.

[9] G. Heins, D. M. Ionel, and M. Thiele, "Winding factors and magnetic fields in permanent-magnet brushless machines with concentrated windings and modular stator cores," *IEEE Trans. Ind. Appl.*, vol. 51, no. 4, pp. 2924–2932, Jul. 2015.

[10] W. Ding, S. Yang, and Y. Hu, "Development and investigation on segmented-stator hybrid-excitation switched reluctance machines with different rotor pole numbers," *IEEE Trans. Ind. Electron.*, vol. 65, no. 5, pp. 3784–3794, May 2018.

[11] Z. Q. Zhu, Z. Azar, and G. Ombach, "Influence of additional air gaps between stator segments on cogging torque of permanent-magnet machines having modular stators," *IEEE Trans. Magn.*, vol. 48, no. 6, pp. 2049–2055, Jun. 2012.
[12] N. J. Baker, D. J. B. Smith, M. C. Kulan, and S. Turvey, "Design and performance of a segmented stator permanent magnet alternator for aerospace," *IEEE Trans. Energy Convers.*, vol. 33, no. 1, pp. 40–48, Mar. 2018.
[13] G. Dajaku and D. Gerling, "A novel 12-teeth/10-poles PM machine with flux barriers in stator yoke," in *Proc. 20th Int. Conf. Elect. Mach.*, Sep. 2012, pp. 36–40.
[14] M.-J. Jin, C.-F. Wang, J.-X. Shen, and B. Xia, "A modular permanent-magnet flux-switching linear machine with fault-tolerant capability," *IEEE Trans. Magn.*, vol. 45, no. 8, pp. 3179–3186, Aug. 2009.
[15] A. S. Thomas, Z. Q. Zhu, and L. J. Wu, "Novel modular-rotor switched-flux permanent magnet machines," *IEEE Trans. Ind. Appl.*, vol. 48, no. 6, pp. 2249–2258, Nov. 2012.
[16] J. T. Chen, Z. Q. Zhu, S. Iwasaki, and R. P. Deodhar, "A novel E-core switched-flux PM brushless AC machine," *IEEE Trans. Ind. Appl.*, vol. 47, no. 3, pp. 1273–1282, May 2011.
[17] R. Owen, Z. Zhu, A. Thomas, G. Jewell, and D. Howe, "Alternate poles wound flux-switching permanent-magnet brushless AC machines," *IEEE Trans. Ind. Appl.*, vol. 46, no. 2, pp. 790–797, Jan. 2010.
[18] I. Petrov, M. Niemela, P. Ponomarev, and J. Pyrhonen, "Rotor surface ferrite permanent magnets in electrical machines: Advantages and limitations," *IEEE Trans. Ind. Electron.*, vol. 64, no. 7, pp. 5314–5322, Jul. 2017.
[19] P. Ponomarev, "Tooth-coil permanent magnet synchronous machine design for special applications," Ph.D. dissertation, Dept. Elect. Eng., Lappeenranta Univ. Technol., Lappeenranta, Finland, 2013.
[20] C. Montoya, J. Tapia, C. Pesce, J. Riedemann, G. Bramerdorfer, and W. Jara, "Electromagnetic analysis of a novel PMSM with modular stator for low power generation," in *Proc. IEEE Int. Conf. Autom./23rd Congr. Chilean Assoc. Autom. Control (ICA-ACCA)*, Oct. 2018, pp. 1–5.
[21] P. Ponomarev, Y. Alexandrova, I. Petrov, P. Lindh, E. Lomonova, and J. Pyrhonen, "Inductance calculation of tooth-coil permanent-magnet synchronous machines," *IEEE Trans. Ind. Electron.*, vol. 61, no. 11, pp. 5966–5973, Nov. 2014.
[22] J. T. Chen and Z. Q. Zhu, "Winding configurations and optimal stator and rotor pole combination of flux-switching PM brushless AC machines," *IEEE Trans. Energy Convers.*, vol. 25, no. 2, pp. 293–302, Jun. 2010.
[23] Y. Li, Q. Lu, and Z.-Q. Zhu, "Unbalanced magnetic force prediction in permanent magnet machines with rotor eccentricity by improved superposition method," *IET Electr. Power Appl.*, vol. 11, no. 6, pp. 1095–1104, Jul. 2017.
[24] H. M. Hamalainen, J. Pyrhonen, J. Nerg, and J. Puranen, "3-D finite element method analysis of additional load losses in the end region of permanent-magnet generators," *IEEE Trans. Magn.*, vol. 48, no. 8, pp. 2352–2357, Aug. 2012.
[25] J. Pyrhonen, T. Jokinen, and V. Hrabovcova, *Design of Rotating Electrical Machines*. New York, NY, USA: Wiley, 2008.

ILYA PETROV received the D.Sc. degree from the Lappeenranta University of Technology (LUT), Finland, in 2015. He is currently a Researcher with the Department of Electrical Engineering, LUT.

CHONG DI was born in Wuxi, China, in 1991. He received the B.Eng. and M.Eng. degrees in electrical engineering from the Hefei University of Technology, Hefei, China, in 2014 and 2017, respectively. He is currently pursuing the Ph.D. degree with the Department of Electrical Engineering, Lappeenranta University of Technology, Finland. His research interest includes high-speed electrical machines.

PIA LINDH born in Helsinki, in 1969. She received the M.Sc. degree in energy technology, in 1998, and the D.Sc. degree in electrical engineering (technology), in 2004, from the Lappeenranta University of Technology (LUT), Lappeenranta, Finland. She is currently an Associate Professor with the Department of Electrical Engineering, LUT Energy, Lappeenranta, where she is engaged in teaching and research of electric motors and electric drives.

MARKKU NIEMELÄ received the B.Sc. degree in electrical engineering from the Helsinki Institute of Technology, Helsinki, Finland, in 1990, and the M.Sc. and D.Sc. degrees in technology from the Lappeenranta University of Technology (LUT), Lappeenranta, Finland, in 1995 and 1999, respectively. He is currently a Senior Researcher with the Carelian Drives and Motor Centre, LUT. His current interests include motion control, control of line converters, and energy efficiency of electric drives.

ANNA-KAISA REPO received the M.Sc. (Eng.) and D.Sc. (Tech.) degrees from the Helsinki University of Technology, Espoo, Finland, in 2004 and 2008, respectively. She is currently a Senior Project Manager of technology platforms with Rocla Oy.

JUHA PYRHÖNEN was born in Kuusankoski, Finland, in 1957. He received the D.Sc. degree from the Lappeenranta University of Technology (LUT), Finland, in 1991. He became an Associate Professor of electrical engineering at LUT, in 1993, and a Professor of electrical machines and drives, in 1997. He is engaged in research and development of electric motors and electric drives. His current research interests include different synchronous machines and drives, induction motors and drives, and solid-rotor high-speed induction machines and drives.